XX ICongresso Brasileiro de Mecânica dos Solos e Engenharia Geotécnica
X Simpósio Brasileiro de Mecânica das Rochas
X Simpósio Brasileiro de Engenheiros Geotécnicos Jovens
24 a 27 de setembro de 2024 – Balneário Camboriú/SC

Influence of Tunnel Depth on Ground Response in Loose and Dense Sandy Soils in Urban Environments

Felipe Paiva Magalhães Vitali
Ph.D. student, Department of Geotechnical Engineering, Engineering School of São Carlos, University of São Paulo, São Carlos, SP, Brazil. felipe.vitali@usp.br

Osvaldo Paiva Magalhães Vitali
Assistant Professor. Department of Civil, Environmental and Construction Engineering, University of Hawaii at Manoa, HI, United States. opmv@hawaii.edu

Tarcisio Barreto Celestino
Professor, Department of Geotechnical Engineering, Engineering School of São Carlos, University of São Paulo, São Carlos, SP, Brazil. tbcelest@usp.br

ABSTRACT: Urban tunnel construction presents significant challenges due to the potential for ground deformations that threaten the integrity of existing buildings and infrastructure. Therefore, the capability to predict such deformations during the design phase is of paramount importance. This paper examines the influence of tunnel depth on deformations induced by Tunnel Boring Machine (TBM) excavations in sandy soils utilizing the Finite Element Method (FEM). The NorSand constitutive model — calibrated against triaxial test data — was selected to capture the complex volumetric and shear behavior of sandy soils under different relative densities. The FEM modeling approach is validated by aligning its predictions with experimental data from six centrifuge tunnel tests reported in the literature. The centrifuge tests were conducted on sands with varying relative densities, tunnel radii, and depths. The paper examines the deformations triggered by shallow tunneling in sandy soils at various depths, assessing the associated risk to overlying structures. Insights from this analysis are critical for the design and planning phases of urban tunneling projects to mitigate the impact above.

KEYWORDS: shallow tunnel, NorSand, numerical modeling, tunnel depth, sand, cohesionless soil.

1 INTRODUCTION

Excavating shallow tunnels in urban areas poses a significant challenge. The tunnel excavation induces deformations in the ground that can damage existing infrastructure. The ratio between tunnel cover (C), the distance from the tunnel crown to the ground surface, and the tunnel diameter (D) heavily affects the induced ground deformations. Celestino and Ferreira (1996) compiled data from the São Paulo metro and used the Gaussian curve (Peck, 1968) to correlate observed building damage with the angular distortion at the ground surface caused by tunnel excavation. Subsequently, the authors associated potential damage to buildings with the C/D ratio and soil volume loss (V_{Ls}), defined as the ratio of the settlement trough area to the tunnel cross-section area. Celestino and Ferreira (1996) showed that shallower tunnels are associated with greater soil volume losses and, consequently, greater building damage.

Similar conclusions to those by Celestino and Ferreira (1996) were drawn from centrifuge tunnel tests, simulating tunnel boring machines (TBMs) under plane strain conditions. Marshall et al. (2012) conducted centrifuge tunnel tests using sand in a very dense state (i.e., relative density of 90%), varying the C/D ratio at 1.3, 2.4, and 4.4. The results showed that shallower tunnels induce greater displacements and narrower settlement troughs and are associated with greater angular distortions and horizontal strains at the ground surface. Franza and Marshall (2019) complemented these findings by studying different relative densities (D_r) and reached the same conclusions regarding the effects of the C/D ratio.

This paper examines the influence of tunnel depth in sandy soils using the Finite Element Method under plane strain conditions. The NorSand constitutive model (Jefferies, 1993) was adopted to properly capture the soil's volumetric behavior. The model was calibrated with triaxial tests under different stress paths and relative densities. The modeling technique used was Volume Loss Control (Addenbroke et al., 1999). The results were validated with six centrifuge test results at different relative densities, depths, and tunnel diameters. With the

validated numerical model, a parametric study was conducted to assess the influence of C/D on the deformations induced at the ground surface.

2 SOIL BEHAVIOR AND FEM MODELING

The centrifuge tunnel tests conducted by Marshall (2009), Farrell (2010), Zhou (2015), and Franza (2016) serve as validation for the developed numerical model. The commercial software Midas GTS NX was used for the numerical analysis. Centrifuge tests offer the convenience of a controlled environment on a centimeter scale and, through centrifugal acceleration, reproduce typical stress states encountered in actual tunnels. The experimental setup consisted of a strongbox, tunnel model, and pressure control system. The strongbox, where the sand is deposited, comprises a U-shaped steel box with an acrylic face. The acrylic face allows displacement measurements using high-precision cameras employing the particle image velocimetry (PIV) technique. Vertical displacement measurements were also taken in the middle of the box using lasers and a linear voltage displacement transducer (LVDT). The tunnel was represented by a brass cylinder wrapped in a latex membrane filled with water. Stress relief is simulated by removing the water from the tunnel model. Marshall (2009), Farrell (2010), Zhou (2015), and Franza (2016) provide more information and details about these centrifuge tests.

Table 1. Calibrated NorSand parameters.

		Remark	**Calibrated parameters**
Critical State Line	Γ	"Altitude" of CSL, defined at 1 kPa	0.97
	λ	Slope of CSL, on base *e*	0.023
Plasticity	M_{tc}	Critical friction ratio for triaxial compression	1.24
	N	Volumetric coupling parameter	0.24
	H	Plastic hardening modulus for loading	75
	χ	Dilatancy parameter	5.7
Elasticity	G_0/p_a	Shear modulus for a reference mean effective stress	500
	m	Exponential stress level dependency of stiffness through parameter	0.5
	ν	Poisson's ratio	0.3

The sand used in all tests was Leighton Buzzard Sand, which is widely applied in experimental practice. Lanzano et al. (2016) present an extensive campaign of laboratory tests on this sand. Based on these tests and parameters in the literature, Vitali (-) and Vitali et al. (-) calibrated the NorSand constitutive model to represent the Leighton Buzzard sand behavior. The NorSand model was developed within the Critical State Mechanics framework, with one of the main inputs being the state parameter (ψ) (Jefferies, 1993), defined as the difference between the current void ratio and the critical void ratio. Thus, the model can represent different states of the sand. Table 1 shows the calibrated parameters of the model and their definition. The initial void ratio is an input, determined according to the target relative density, while the other parameters remain constant regardless of soil relative density. Figure 1 shows the results of compression and extension triaxial tests for different relative densities (D_r) from laboratory tests (Lanzano et al., 2016) and numerical simulations. The numerical predictions and the experimental observations show excellent agreement.

Figure 2 shows the finite element mesh. The FEM modeling approach followed the recommendations by Vitali et al. (2018a, 2021a) and Vitali et al., (2024). These procedures led to excellent numerical results in the validations of analytical solutions (Vitali et al., 2018b; 2019a; 2019b; 2019d; 2020a; 2020b; 2020c; 2021b; 2022a) and simulating case histories (Vitali et al., 2019c; 2021c). The model dimensions were adopted for the prototype scale. Symmetry was utilized by discretizing only half of the model. Second-order elements (i.e., quadratic interpolation) were adopted, ensuring quality results even under high nonlinearity, as Vitali et al. (2024) demonstrated. The volume loss control (Addenbroke et al., 1999) numerical technique was adopted, which involves a gradual reduction of nodal forces around the tunnel perimeter, and stress relief is associated with tunnel volume loss from the tunnel deformation. This is a suitable technique to simulate the centrifuge tunnel test.

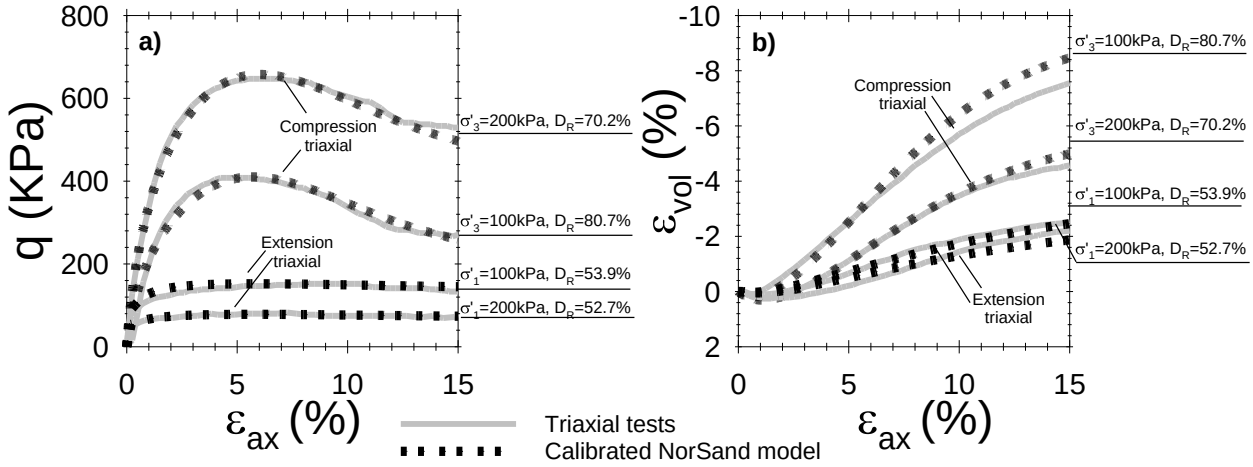

Figure 1. Comparison between results of triaxial tests (Lanzano et al., 2016) on Leighton Buzzard Sand and the NorSand constitutive model. Results expressed in deviatoric stress variation (a) and volumetric strain (b) with the evolution of axial deformation.

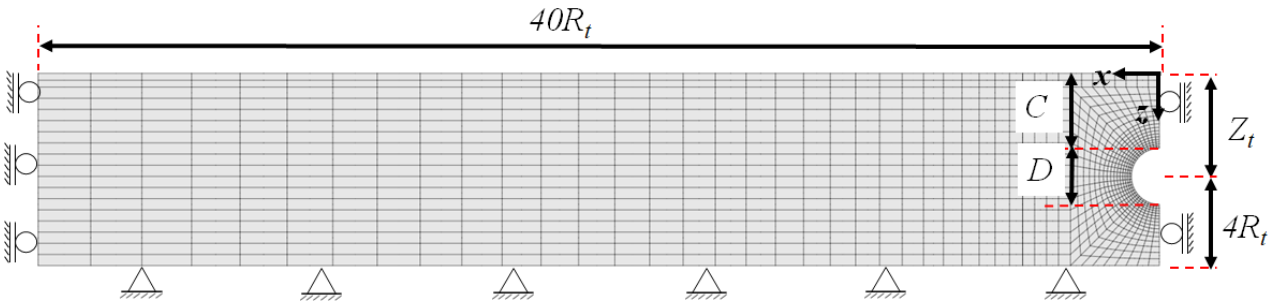

Figure 2. Plane strain finite element mesh for a tunnel with diameter D, radius R_t, cover C, and depth Z_t.

Figure 3 compares the results of the developed numerical model with experimental results conducted by Farrell (2010), with C/D=1.3, D=6.15m, and D_r=90%, and Marshall (2009), with C/D=2.4, D=4.65m, and D_r=90%. Figures 3a and b show the settlement trough normalized by the tunnel radius (R_t) obtained in the FEM models and in the centrifuge tunnel tests from PIV and laser measurements. The Yield Density (Celestino and Ruiz, 1997; Celestino et al., 2000) curve was used to adjust the settlement trough from laser data. Figure 3c illustrates the evolution of the normalized vertical displacement (S_v) at the ground surface along the tunnel centerline in relation to the evolution of tunnel volume loss. The results presented in Figure 3 demonstrate that the numerical model reproduced the behaviors observed in the physical experiment. The model also captured the nonlinear evolution of maximum displacement associated with the dilatant behavior of the soil, as shown in Figure 3c. A comprehensive discussion of the presented results can be found in Vitali (-) and Vitali et al. (-).

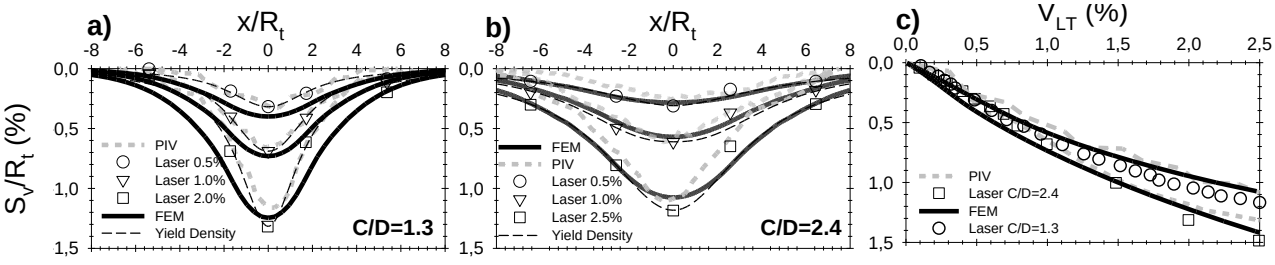

Figure 3. Comparison between centrifuge and numerical model results for settlement troughs (a and b) and evolution of vertical displacement at the surface along the tunnel's centerline with tunnel volume loss (c).

3 GROUND DISPLACEMENTS AND DAMAGE

In this section, a parametric study is conducted with the validated numerical model to assess the influence of tunnel cover on induced displacements and surface damage. The study is structured by fixing the tunnel diameter at 10m and the relative density of the sand at 30% and 90%. The tunnel cover varies at 10m, 20m, and 30m, resulting in *C*/*D* ratios of 1, 2, and 3, typical of tunnels in urban environments.

Figures 4 and 5 provide information on induced surface displacements. Figure 4 displays vertical and horizontal displacements on the soil surface for loose sand (D_r=30%, depicted on the left side of the graph) and dense sand (D_r=90%, depicted on the right side). These displacements correspond to tunnel volume losses of 0.5%, 1%, and 2.5%. Positive horizontal displacements indicate movement toward the tunnel's center, while negative vertical displacements indicate downward movement.

Figure 4 shows that for small tunnel volume losses, specifically 0.5%, the magnitudes of horizontal and vertical displacements are relatively small for both soil relative densities. However, the settlement troughs and horizontal displacement profiles are significantly wider for deeper tunnels (*C*/*D*=3) than for shallower tunnels (*C*/*D*=1). As the tunnel volume loss increases, the contrasts in displacement magnitudes for different *C*/*D* ratios and relative densities become more pronounced. For high tunnel volume losses, the effect of soil dilatancy is more pronounced, and the displacements in dense sands are significantly smaller than in loose sands, as discussed by Vitali et al. (-) and Vitali (-).

As Figure 4 indicates, shallower tunnels produce larger displacements with narrower settlement troughs. Consequently, greater angular distortions and horizontal deformations are mobilized in these tunnels, implying a higher risk of structural damage to adjacent infrastructure. On the other hand, deeper tunnels, although causing less intense deformations, can affect a wider range of buildings due to more spread-out displacements.

Figure 5 depicts the evolution of normalized settlement at the ground surface along the tunnel centerline (S_v/R_t) relative to the tunnel volume loss. The results for loose sand are presented in Figure 5a, while Figure 5b shows the results for dense sand. The maximum displacement evolves almost linearly for loose sand, while nonlinearity substantially increases as the relative density increases from 30% to 90%. This behavior is consistent across all analyzed cover-to-diameter ratios (C/D=1, 2, 3). The observed trends are consistent with the centrifuge tunnel test results presented by Franza and Marshall (2019).

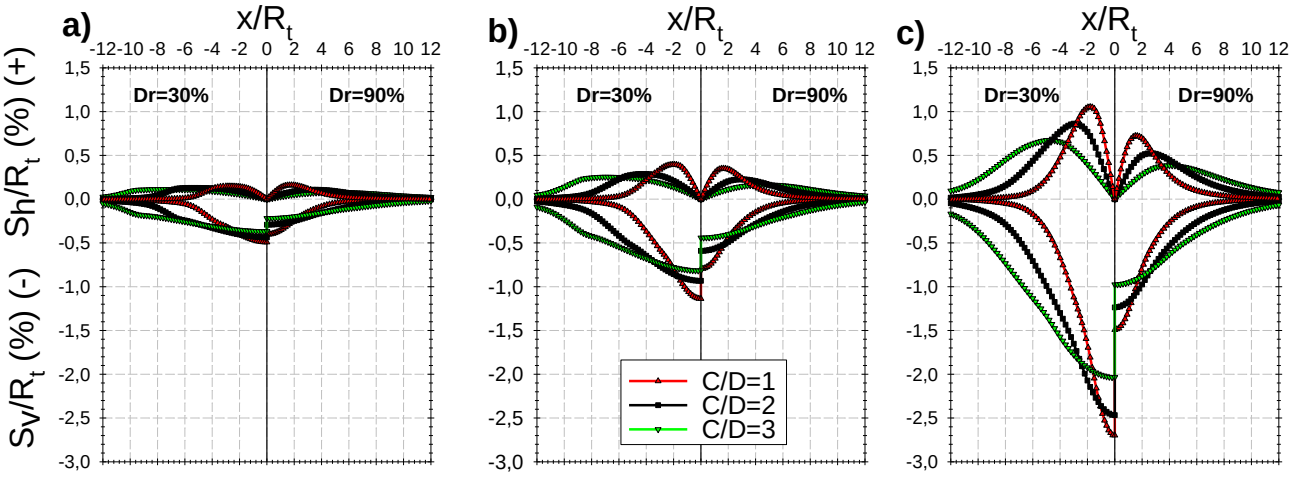

Figure 4. Normalized settlement trough for dense (Dr=90%) and loose (Dr=30%), for different C/D (1, 2 and 3), and different tunnel volume loss, 0,5% (a), 1,0% (b) and 2,5% (c).

In Tunnel Engineering practice, horizontal displacements at the ground surface are often estimated from vertical displacements measured during tunnel construction by imposing the displacement vector direction. For constant-volume deformations (i.e., undrained behavior), it is generally assumed that the displacement vector direction intersects the tunnel centerline at the same point, following O'Reilly and New (1982) and Taylor (1995). Figure 6a shows the intersection between the tunnel centerline and the trajectory of the displacement vector at a point over the ground surface. The parameters of the Sh/Sv=x/Zv relationship are as

follows: Sh and Sv are horizontal and vertical displacements, respectively; Zv is the depth of intersection between the trajectory of the displacement vector and the tunnel centerline; Zt is the tunnel depth.

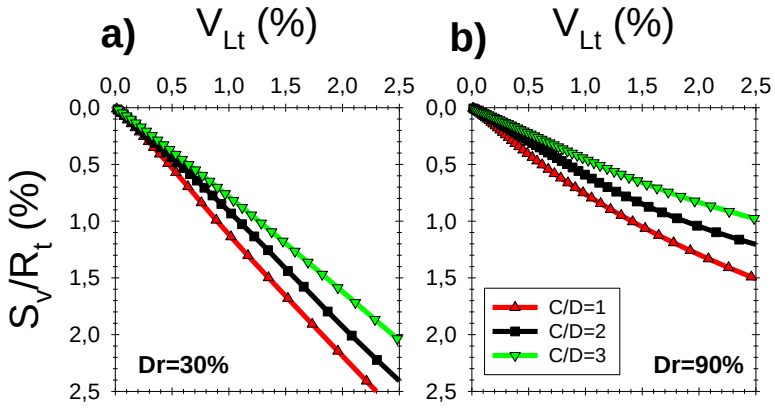

Fig. 5 Normalized surface settlement above tunnel crown (a) and trough width parameter (b) evolution with tunnel volume loss.

Figure 6 illustrates the normalized depth, Z_v/Z_t, as a function of the normalized distance to the tunnel axis, x/R_t. The results for the analyzed cases (C/D=1, 2, and 3; D_r=30% and 90%) for tunnel volume losses of 0.5% and 2.5%. The proposals for clayey soils (undrained behavior) made by O'Reilly and New (1982) and Taylor (1995) are included for reference. These proposals are based on a constant Z_v/Z_t ratio along x/R_t.

From Figures 6b and 6c, it is noted that the values of Z_v/Z_t substantially depend on the distance to the tunnel axis (x), the relative density of the soil (D_r), the tunnel volume loss (V_{Lt}), and the cover-to-diameter ratio (C/D). As shown, Zv/Zt amplifies as x/Rt increases, indicating that the trajectory of the displacement vector intersects the tunnel centerline at progressively deeper points. This trend becomes more pronounced in shallower tunnels. For C/D = 3, the variation of Z_v/Z_t with x/R_t decreases, suggesting that Z_v/Z_t may stay approximately constant with x/R_t for deep tunnels, given a specific tunnel volume loss.

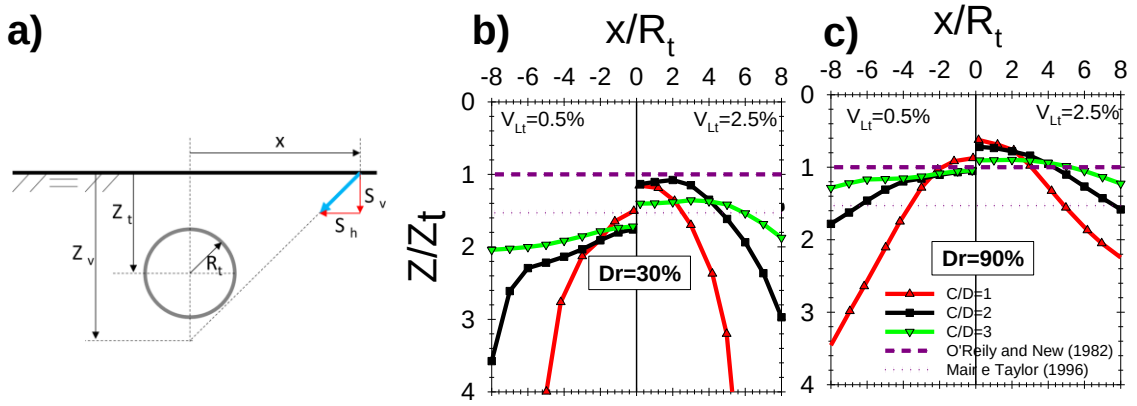

Figure. 6 (a) Sketch of the intersection between the tunnel centerline and the displacement vector's trajectory at depth Z_v. (b) and (c) Normalized depth (Z_v/Z_t) versus the normalized distance from the tunnel axis (x/R_t) for tunnel volume losses of 0.5% and 2.5% for loose (b) and very dense sand (c).

Tunnels in urban environments interact with various structures, each with differing stiffness, foundation types, and states of conservation, making it essential to analyze potential damage to buildings in the early stages of the project. It is well-known that the structures will affect the ground deformations surrounding the tunnel. As shown by Potts and Addenbroke (1997), rigid structures will behave more like a rigid body, reducing angular distortions and horizontal deformations, while flexible structures will behave closer to the greenfield condition. Thus, in practice, potential damage to buildings is first assessed under greenfield conditions, a conservative approach. If these analyses predict larger ground surface deformations, more detailed studies that consider the presence of buildings should be conducted.

Boscardin and Cording (1989) and Son and Cording (2005) recommend using the principal strain (ε_p) resulting from tunnel excavations to assess potential damage to buildings. The principal strain is the result of the combination of angular distortion (β) and horizontal strains (ε_h):

$$\varepsilon_p = \varepsilon_h \cos^2 \theta_{max} + \beta \sin \theta_{max} \cos \theta_{max} \quad \text{Eq. 1}$$

Where θ_{max} is the angle that maximizes ε_p: $\tan 2\theta_{max} = |\beta / \varepsilon_h|$.

Son and Cording (2005) provided limits for principal strain magnitudes associated with building damage effects. The proposed strain limits for damage categories are as follows: negligible for $\varepsilon_p < 0.075\%$, slight for $0.075\% < \varepsilon p < 0.167\%$, moderate to severe for $0.167\% < \varepsilon p < 0.333\%$, and very severe for $\varepsilon_p > 0.333\%$. These limits, based on real tunnel experiences and modeling of soil-structure interactions for masonry buildings on shallow foundations, are widely accepted both in academic literature and tunnel design practices.

Figure 7 illustrates the relationship between angular distortion (β) and the corresponding horizontal tensile strain (ε_h) at the maximum principal strain on the ground surface. This is shown for cover-to-diameter ratios of 1, 2, and 3 and relative densities of 30% (loose sand) and 90% (dense sand). A total of 10 data points, with tunnel volume loss ranging from 0.25% to 2.5%, are plotted for each scenario. The designated regions I, II, and III align with the damage classifications proposed by Son and Cording (2005). Specifically, Region I corresponds to expected slight damages to buildings; Region II, moderate to severe damages; and Region III, very severe damages.

Interestingly, the correlation between angular distortion and horizontal tensile strain appears almost linear across all cover-to-diameter ratios and relative densities analyzed. This trend falls within the bounds established by Boscardin and Cording (1989) based on historical case studies. By performing linear regression with the data points, the horizontal tensile strain is approximately 0.67 times the angular distortion, regardless of C/D, Dr, and VLt values.

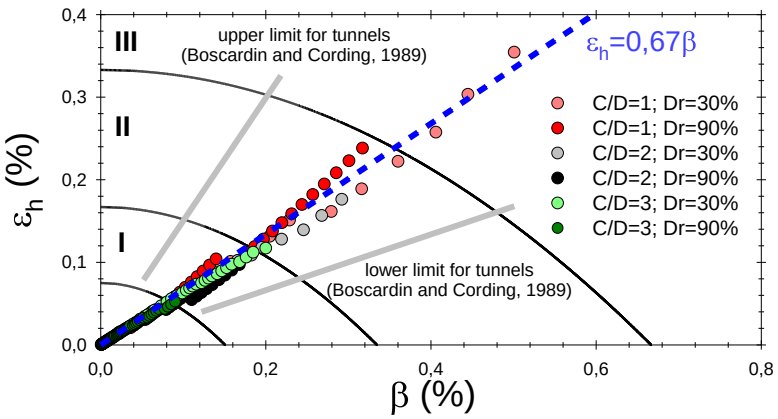

Figure 7. Strain paths, angular distortion versus horizontal deformation, for analyzed cases (C/D=1, 2, and 3; Dr=30% and 90%)

5 CONCLUSION

This paper assesses the influence of the cover-to-diameter ratio (C/D) on tunnel excavation in cohesionless soils. A finite element model was developed and validated with centrifuge tunnel testing results. The NorSand constitutive model was chosen and calibrated with triaxial compression and extension tests at different relative densities for the same sand used in the centrifuge tunnel tests. Excellent agreement between experiments and numerical models was observed. With the validated numerical model, parametric analyses were conducted for cover-to-diameter ratios, C/D, of 1, 2, and 3, diameter (D) of 10m, and relative densities (Dr) of 30% and 90%.

As expected, shallower tunnels induced larger displacements and narrower settlement troughs, thus presenting a higher risk of damage to buildings. However, deeper tunnels produce deformations in a substantially wider area.

The ratio of normalized depth Z_v/Z_t, representing the depth where the displacement vector's trajectory intersects the tunnel centerline (Z_v) in relation to the tunnel's depth (Zt), is significantly affected by factors such as relative density, tunnel volume loss, and proximity to the tunnel centerline. Thus, adopting a fixed Z_v/Z_t ratio to estimate horizontal displacements in shallow tunnels within sandy ground, as suggested by O'Reilly and New (1982), should produce inaccurate predictions.

The correlation between angular distortion (β) and tensile horizontal strain (ε_h) at the point of maximum principal strain exhibits a nearly linear pattern as the tunnel volume loss increases, unaffected by factors like cover-to-diameter ratio (C/D) and soil relative density (Dr). Notably, the tensile horizontal strain constitutes approximately 67% of the angular distortion. In tunnel practice, buildings are typically included in analyses only when greenfield surface deformations exceed the thresholds specified by Son and Cording (2005). Therefore, the relationship between β and ε_h enhances the predictions of potential damage to buildings due to tunnel excavation in sandy soils.

ACKNOWLEDGMENTS

The authors acknowledge the support provided by the Brazilian government's research funding agency, CNPq (Conselho Nacional de Desenvolvimento Cientifico), Contract 162113/2020-0: Post-Doctoral Scholarship, and CAPES (Coordenação de Aperfeiçoamento de Pessoal de Nível Superior). The authors also thank Midas Information Technology Co. Ltd. for providing the license for the Midas GTS NX software utilized in this research.

REFERENCES

Addenbrooke, T. I., Potts, D. M., & Puzrin, A. M. (1997). *The influence of pre-failure soil stiffness on the numerical analysis of tunnel construction*. Géotechnique, 47(3), 693-712.

Boscardin, M. D., and Cording, E. J. (1989). *Building response to excavation-induced settlement*. Journal of Geotechnical Engineering, 115(1), 1-21.

Celestino, T. B. and Ruiz, A. P. T. (1998). *Shape of settlement troughs due to tunneling through different types of soft ground*. Felsbau, 16, 118–121.

Celestino, T. B. and Ferreira, A. A. (1996). *Building damage associated with recent tunnels excavated for the São Paulo subway*. Proc. North American Tunneling '96 Vol. 1, 81-88, Rotterdam: A. A. Balkema.

Celestino, T. B., Gomes, R. A. M. and Bortuluci, A. A. (2000). *Errors in ground distortions due to settlement trough adjustment*. Tunnelling and Underground Space Technology, 15(1), 97–100.

Farrell, R. P. (2010). *Tunnelling in sands and the response of buildings* (PhD Thesis). University of Cambridge. Cambridge, UK.

Franza, A. (2016). *Tunnelling and its effects on piles and piled structures* (PhD Thesis). University of Nottingham. Nottingham, UK.

Franza, A., Marshall, A. M. and Zhou, B. (2019). *Greenfield tunnelling in sands: The effects of soil density and relative depth*. Géotechnique. 69. 297-307. 10.1680/jgeot.17.p.091.

Jefferies, M. G. (1993). *Nor-Sand: a simple critical state model for sand*. Géotechnique, 43(1), 91-103.

Lanzano, G., Visone, C., Bilotta, E. and Santucci de Magistris, F. (2016). *Experimental Assessment of the Stress–Strain Behaviour of Leighton Buzzard Sand for the Calibration of a Constitutive Model*. Geotechnical and Geological Engineering. 34. 10.1007/s10706-016-0019-5.

Marshall, A. (2009). *Tunnelling in sand and its effect on pipelines and piles* (PhD Thesis). University of Cambridge. Cambridge, UK

Marshall, A. M., Farrell, R., Klar, A. & Mair, R. (2012*). Tunnels in sands: the effect of size, depth and volume loss on greenfield displacements*. Géotechnique 62, No. 5, 385–399, https://doi.org/10.1680/geot.10.P.047.

O'Reilly, M. P. and New, B. M. (1982). *Settlements above tunnels in the United Kingdom - their magnitude and prediction*. Tunnelling '82, Papers Presented at the 3rd International Symposium. Inst of Mining and Metallurgy, London, England, Brighton, England.

Potts, D. M., & Addenbrooke, T. I. (1997). A structure's influence on tunnelling-induced ground movements. Proceedings of the Institution of Civil Engineers-Geotechnical Engineering, 125(2), 109-125.

Son, M., and Cording, E. J. (2005). *Estimation of building damage due to excavation-induced ground movements*. Journal of geotechnical and geoenvironmental engineering, 131(2), 162-177.

Taylor, R.N. (1995). *Tunnelling in soft ground in the U K*. Underground Construction in Soft Ground (eds. K. Fujita and O. Kusakabe), Balkema, pp.123-126.

Zhou, B. (2014). *Tunnelling-induced ground displacements in sand* (PhD Thesis). University of Nottingham. Nottingham, UK.

Vitali, F. P. M; (2024). *Deformations caused by tunnel excavation in sandy ground (in portuguese)*. Master's dissertation. São Carlos School of Engineering, University of São Paulo. In preparation.

Vitali, F. P. M; Vitali, O. P. M.; Celestino T. B.; Bobet, A. (2024) *FEM modeling requirements for accurate highly nonlinear shallow tunnels analysis*. Soil and Rocks. 47(1). 10.28927/SR.2024.000923.

Vitali, F. P. M; Vitali, O. P. M.; Celestino T. B.; Bobet, A. (-) *Impact of Relative Density on Shallow TBM Tunnel Excavation: Ground Behavior and Building Damage Risks*. *In review*.

Vitali, O. P. M., Celestino, T. B., & Bobet, A. (2018a). *3D finite element modeling optimization for deep tunnels with material nonlinearity*. Undergr. Sp., 3(2):125–139. https://doi.org/10.1016/j.undsp.2017.11.002

Vitali, O.P.M., Celestino, T.B., & Bobet, A., (2018b). *Analytical solution for tunnels not aligned with geostatic principal stress directions*. Tunn. Undergr. Sp. Technol. 82, 394–405. https://doi.org/10.1016/j.tust.2018.08.046.

Vitali, O. P. M., Celestino, T. B., & Bobet, A. (2019a) *Shallow tunnel not aligned with the geostatic principal stress directions*. In: Proceedings of Geo-Congress2019, GSP, 313:214-222. https://doi.org/10.1061/9780784482155.023

Vitali, O. P. M., Celestino, T. B., & Bobet, A. (2019b) *Shallow tunnels misaligned with geostatic principal stress directions: analytical solution and 3D face effects*. Tunn. Undergr. Sp. Technol., 89: 268-283. https://doi.org/10.1016/j.tust.2019.04.006

Vitali, O.P.M., Celestino, T.B., & Bobet, A., (2019c). *Progressive failure due to tunnel misalignment with geostatic principal stresses*. In: Proceedings of ISRM 14th International Congress on Rock Mechanics, pp. 2292-2299.

Vitali, O. P. M., Celestino, T. B., & Bobet, A. (2019d). *Buoyancy effect on shallow tunnels*. International Journal of Rock Mechanics and Mining Sciences, 114, 1–6. https://doi.org/10.1016/j.ijrmms.2018.12.012

Vitali, O.P.M., Celestino, T.B., & Bobet, A., (2020a). *Analytical solution for a deep circular tunnel in anisotropic ground and anisotropic geostatic stresses*. Rock Mech. Rock Eng. 53 (9), 3859–3884. https://doi.org/10.1007/s00603-020-02157-5

Vitali, O.P.M., Celestino, T.B., & Bobet, A., (2020b). *Tunnel misalignment with geostatic principal stress directions in anisotropic rock masses*. Soils and Rocks, Soils and Rocks, São Paulo, 43(1), 123-138, January-March, 2020, https://doi.org/10.28927/SR.431123.

Vitali, O.P.M., Celestino, T.B., & Bobet, A., (2020c). *Deformation patterns and 3D face effects of tunnels misaligned with the geostatic principal stresses in isotropic and anisotropic rock masses*. 54th US Rock Mechanics /Geomechanics Symposium (ARMA 2020).

Vitali, O. P. M., Celestino, T. B., & Bobet, A. (2021a). *New modeling approach for tunnels under complex ground and loading conditions*. Soils and Rocks 44 (1), 1–8. https:// doi.org/10.28927/SR.2021.052120.

Vitali, O.P.M., Celestino, T.B., Bobet, A., (2021b). *Behavior of tunnels excavated with dip and against dip*. Underground Space 6 (6), 709–717. https://doi.org/10.1016/j. undsp.2021.04.001.

Vitali, O. P. M., Celestino, T. B., & Bobet, A. (2021c). *Construction strategies for a NATM tunnel in São Paulo, Brazil, in residual soil*. Underground Space, 7(1):1-18. https://doi.org/ 10.1016/j.undsp.2021.04.002.

Vitali, O. P. M., Celestino, T. B., & Bobet, A. (2022). *3D face effects of tunnels misaligned with the principal directions of material and stress anisotropy*. Tunnelling and Underground Space Technology, 122, 104347. https://doi.org/10.1016/j.tust.2021.104347